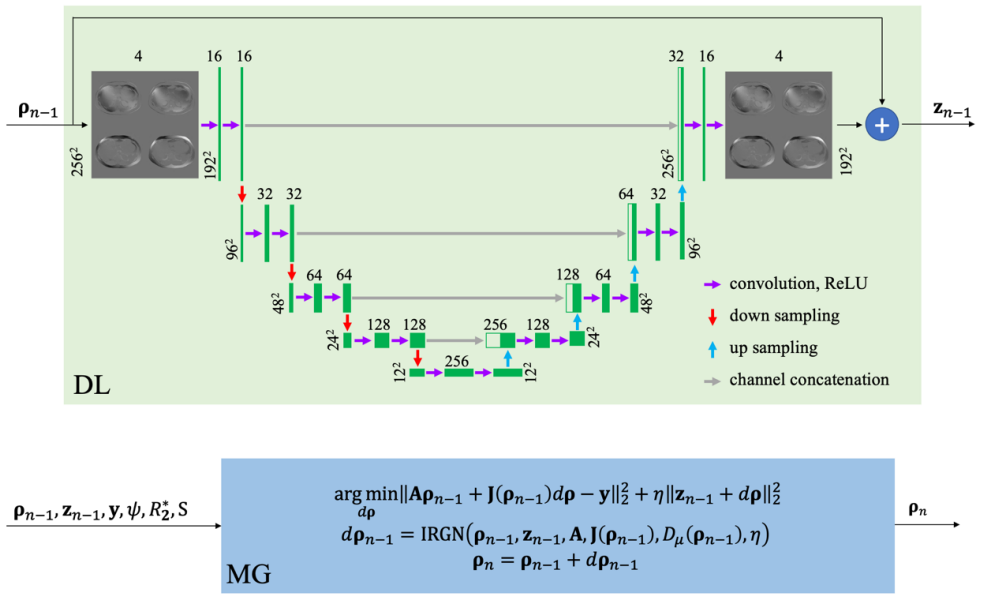

Figure S1 The structure of the DL block and MG block in the n-th outer iteration in the model-guided reconstruction block. DL block contains a five-layer modified residual U-net network. MG block contains a conjugate gradient block for solving the sub-problem. DL, deep learning; MG, model-guided; IRGN, iteratively regularized Gauss-Newton algorithm.

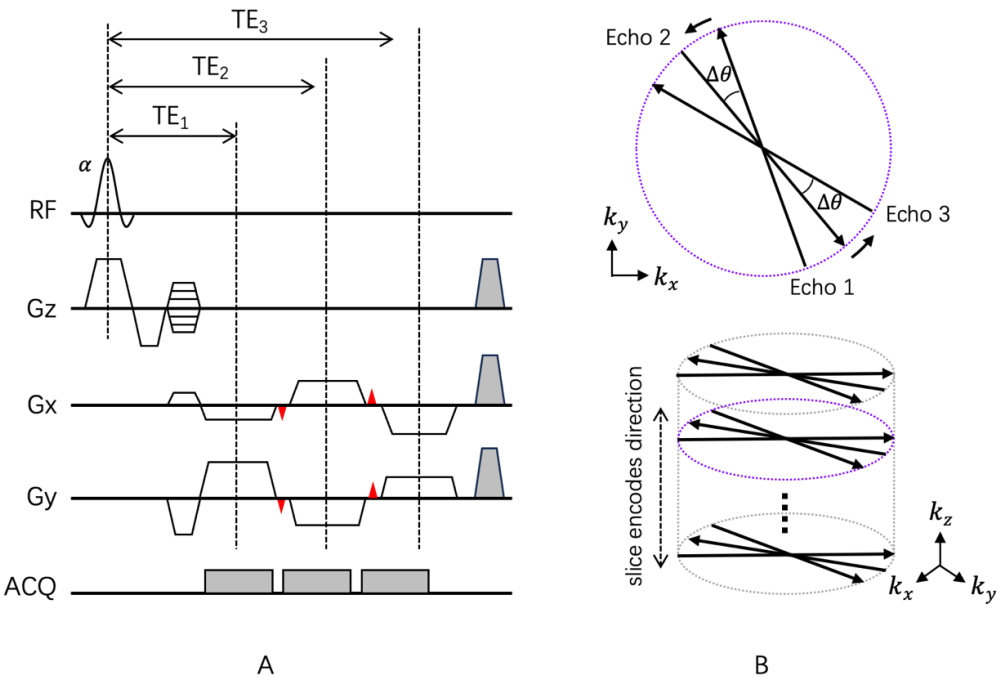

Figure S2 Diagram of the 3D blipped golden-angle stack-of-stars multi-gradient-echo pulse sequences and the corresponding k-space sampling trajectories. (A) Blip gradients represented by the red triangles are inserted between the readout gradients of the echo train. (B) The multi-echo data acquisition strategy and the corresponding k-space trajectories. RF, radio frequency; ACQ, acquisition module; 3D, three-dimensional.

https://dx.doi.org/10.21037/qims-23-1396

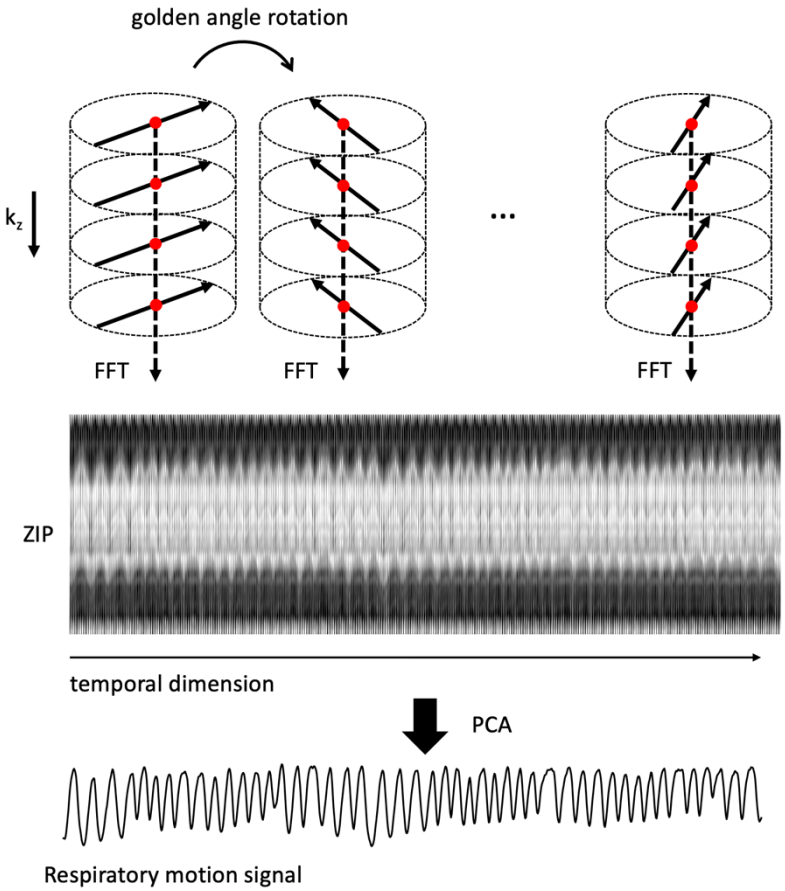

Figure S3 Flow chart of the respiratory motion extraction using the golden-angle stack-of-stars sequence. The ZIP profiles were computed by performing 1D Fourier transform of the center points along slice direction. Respiratory motion detection was then performed using PCA. The principal component with highest peak in the frequency range of 0.1 ~ 0.5 Hz was selected to represent the respiratory motion. FFT, fast Fourier transform; ZIP, z-intensity projection; PCA, principal component analysis.

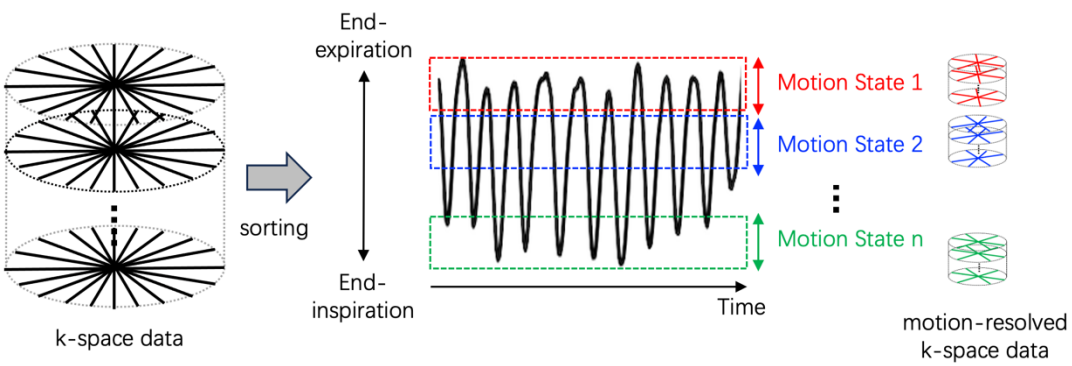

Figure S4 Flow chart of the k-space data sorting. The acquired radial k-space data are sorted into different respiratory motion states (bins) from expiration (top) to inspiration (bottom). Dashed boxes with different colors indicate different motion states. In this study, the number of spokes sorted in each motion state is the same.

https://dx.doi.org/10.21037/qims-23-1396

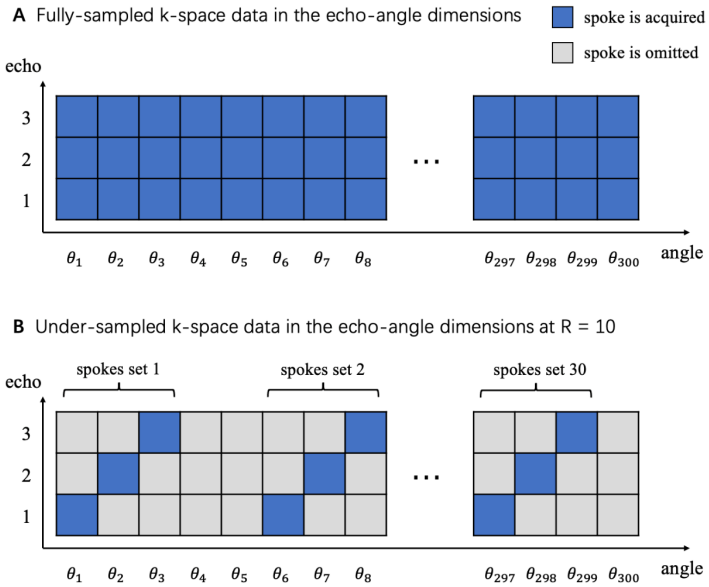

Figure S5 Diagram of the k-space data acquisition along the echo dimension. (A) Fully-sampled k-space data in the echo-angle dimensions. (B) Undersampled k-space data in the echo-angle dimensions at R=10. The blue or gray blocks represent the acquired or omitted spokes in the echo-angle dimension, respectively. The horizontal coordinate indicates the angle of the acquired spoke in kx-ky plane.

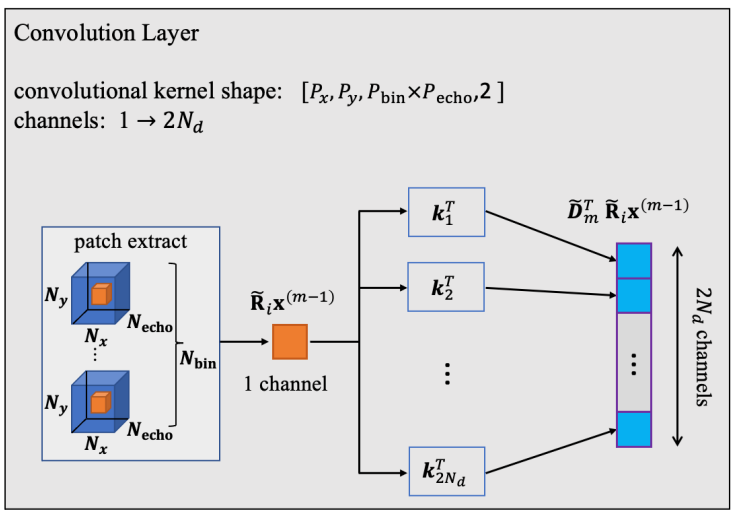

Figure S6 Diagram of the relationship between the convolution layer and the $\tilde{\boldsymbol{D}}_m^T\,\tilde{\mathbf{R}}_i\mathbf{x}^{(m-1)}$ operation in ISTA. A high-dimensional convolution layer with the convolutional kernel shape of $\left[P_x, P_y, P_{bin} \times P_{\text{echo}}, 2\right]$, 1 input channel, and $2N_d$ output channels. This layer contains $1 \times 2N_{\text{d}}$ convolutional kernels where the j-th kernel is represented by $\boldsymbol{k}_i \in \mathbb{R}^{P_x P_y P_{bin} \times P_{echo}, 2}$. Then these kernels were performed on a single channel dynamic multi-echo image tensor $\mathbf{x}^{(m-1)}$, each calculation of the convolutional kernel $\boldsymbol{k}_j$ at a given patch $\tilde{\mathbf{R}}_i\mathbf{x}^{(m-1)}$ can be expressed as $\boldsymbol{k}_j^T\left(\tilde{\mathbf{R}}_i\mathbf{x}^{(m-1)}\right)$. Assigning the weights of the convolutional kernel as $\tilde{\boldsymbol{D}}_m = \left(\boldsymbol{k}_1, \boldsymbol{k}_2, \cdots, \boldsymbol{k}_{2Nd}\right)$, then the $2N_d$-dimensional features can be expressed by $\tilde{\boldsymbol{D}}_m^T\tilde{\mathbf{R}}_i\mathbf{x}^{(m-1)}$, which is equivalent to the transpose of the dictionary matrix applied on the extracted patches $\tilde{\mathbf{R}}_i\mathbf{x}^{(m-1)}$ ISTA, iterative soft thresholding algorithm.

https://dx.doi.org/10.21037/qims-23-1396

Table S1 Quantitative results for CS-WF, PNCRNN, and HMDDL at R=6 on five test healthy subjects and five test NAFLD subjects

Metrics	Healthy			NAFLD		
	CS-WF	PNCRNN	HMDDL	CS-WF	PNCRNN	HMDDL
PSNR (dB)	39.72±3.71	44.71±2.05	47.30±3.06	40.76±2.98	45.45±1.82	48.10±1.69
SSIM	0.968±0.025	0.988±0.004	0.993±0.004	0.971±0.023	0.989±0.004	0.993±0.003
RMSE	0.0114±0.0059	0.0060±0.0014	0.0047±0.0035	0.0097±0.0036	0.0055±0.0011	0.0040±0.0010

The PSNR, SSIM, and RMSE values are presented as mean ± standard deviations. CS-WF, compressed sensing-based water-fat separation; PNCRNN, parallel non-Cartesian convolutional recurrent neural networks; HMDDL, high-dimensional model-guided deep dictionary learning; NAFLD, nonalcoholic fatty liver disease; PSNR, peak signal-to-noise ratio; SSIM, structure similarity; RMSE, root mean squared error.

Table S2 Quantitative results for CS-WF, PNCRNN, and HMDDL at R=8 on five test healthy subjects and five test NAFLD subjects. The PSNR, SSIM, and RMSE values are presented as mean ± standard deviations.

Metrics	Healthy			NAFLD		
	CS-WF	PNCRNN	HMDDL	CS-WF	PNCRNN	HMDDL
PSNR (dB)	37.17±3.37	44.40±2.65	46.30±2.97	37.70±2.97	44.93±1.51	46.99±1.85
SSIM	0.944±0.046	0.987±0.005	0.991±0.004	0.954±0.038	0.987±0.004	0.992±0.003
RMSE	0.0150±0.0066	0.0064±0.0034	0.0053±0.0035	0.0139±0.0052	0.0058±0.0010	0.0046±0.0010

CS-WF, compressed sensing-based water-fat separation; PNCRNN, parallel non-Cartesian convolutional recurrent neural networks; HMDDL, high-dimensional model-guided deep dictionary learning; NAFLD, nonalcoholic fatty liver disease; PSNR, peak signal-to-noise ratio; SSIM, structure similarity; RMSE, root mean squared error.

Table S3 P values of the paired t-test for CS-WF and HMDDL at R=6 on five test healthy subjects and five test NAFLD subjects

Metrics	Healthy			NAFLD		
	CS-WF	PNCRNN	HMDDL	CS-WF	PNCRNN	HMDDL
Paired *t*-test for PDFF	0.0013	0.5721†	0.7827†	0.9361†	0.9836†	0.9970†
Paired *t*-test for R_2^*	0.3881†	0.9560†	0.9974†	0.8059†	0.9773†	0.9953†

†, the paired *t*-tests which do not reject the null hypothesis, indicating that there is no significant difference between the measurements and the reference values. CS-WF, compressed sensing-based water-fat separation; PNCRNN, parallel non-Cartesian convolutional recurrent neural networks; HMDDL, high-dimensional model-guided deep dictionary learning; NAFLD, nonalcoholic fatty liver disease; PDFF, proton-density fat fraction.

Table S4 P values of the paired *t*-test for CS-WF and HMDDL at R=8 on five test healthy subjects and five test NAFLD subjects.

Metrics	Healthy			NAFLD		
	CS-WF	PNCRNN	HMDDL	CS-WF	PNCRNN	HMDDL
Paired *t*-test for PDFF	<0.01	0.7061†	0.5354†	0.9121†	0.9846†	0.9945†
Paired *t*-test for R_2^*	0.4077†	0.9739†	0.9946†	0.9170†	0.9387†	0.9600†

†, the paired *t*-tests which do not reject the null hypothesis, indicating that there is no significant difference between the measurements and the reference values. CS-WF, compressed sensing-based water-fat separation; PNCRNN, parallel non-Cartesian convolutional recurrent neural networks; HMDDL, high-dimensional model-guided deep dictionary learning; NAFLD, nonalcoholic fatty liver disease; PDFF, proton-density fat fraction.

https://dx.doi.org/10.21037/qims-23-1396